Evaluation of APD and SiPM Matrices as Sensors for Monolithic PET Detector Blocks

P. García de Acilu, P. Rato Mendes, *Member, IEEE*, M. Cañadas, I. Sarasola, R. Cuerdo, L. Romero, C. Willmott

Abstract–**Gamma detectors based on monolithic scintillator blocks coupled to APDs matrices have proved to be a good alternative to pixelated ones for PET scanners. They provide comparable spatial resolution, improve the sensitivity and make easier the mechanical design of the system. In this study we evaluate by means of Geant4-based simulations the possibility of replacing the APDs by SiPMs. Several commercial matrices of light sensors coupled to LYSO:Ce monolithic blocks have been simulated and compared. Regarding the spatial resolution and linearity of the detector, SiPMs with high photo detection efficiency could become an advantageous replacement for the APDs.**

I. INTRODUCTION

WE are developing a BrainPET insert for existing MRI equipment, based on annihilation gamma detection using monolithic blocks of cerium-doped lutetium yttrium orthosilicate (LYSO:Ce), coupled to arrays of commercial avalanche photodiodes (APDs) [1]. The scintillation light generated in the monolithic block reaches the sensor pixels with a distribution which depends on the incidence point of the gamma on the block surface and on the incidence angle. The entrance coordinates over the block surface are extracted from the measured signals by means of neural networks positioning algorithms [2], while the incidence angle is estimated from the relative position in the ring of the two detectors triggering in coincidence. The determination of both values, for the two detectors giving the coincidence, provides enough knowledge to fully determine the PET Lines-of-Response (LoRs), without parallax errors (Fig. 1 left). The suitability of these sensors for our system has been checked in previous studies by means of simulations [3], and validated experimentally [4].

A possible future upgrade could be to replace the APDs with commercial arrays of silicon photomultipliers (SiPMs). These devices consist of a series of APD micro-cells, being each cell an independently biased Geiger-mode detector. When a photon interacts in one cell, it discharges through an individual quenching resistor which is connected to a common output. Since the response of each cell behaves as a binary signal, the total output of the SiPMs is proportional to the number of photons interacting in the micro-cells. SiPMs are magnetically compatible devices, just like the APDs, but they
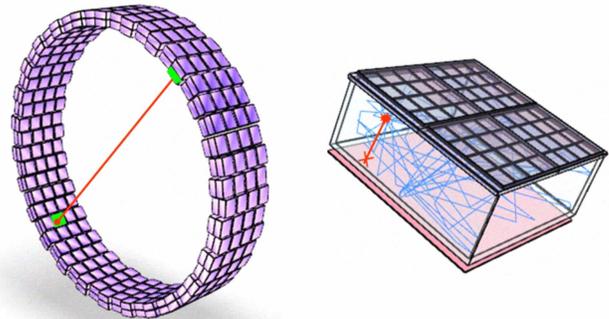
Fig. 1. Left: LoR defined by the relative position of the blocks and the incidence points estimated over their surfaces. Right: Light distribution generated into a monolithic block by a gamma emitted from a flat source placed near the entrance surface.

TABLE I
GEOMETRICAL CHARACTERISTICS OF THE COMMERCIAL MATRICES

	APDs (Hamamatsu)	SiPMs (SensL)	MPPC (Hamamatsu)
Crystal surface (mm^2)	18.5×21.4	26.2×26.2	26×26
Pixel active area (mm^2)	1.6×1.6	2.85×2.85	3×3
Microcell area (μm^2)	---	35×35	50×50
Nr of microcells per pixel	---	3640	3600

provide some advantages such as an excellent timing resolution, below 1 ns, and a typical intrinsic gain of 10^5-10^7.

In this simulation study we present a comparison of the spatial resolution and linearity of several detector devices consisting of one monolithic block read with different commercial matrices of light sensors.

II. SIMULATED DETECTOR AND SENSOR GEOMETRY

Simulations have been carried out with GAMOS 2.0.2, a Geant4-based simulation software developed at CIEMAT [5]. Three cases were simulated depending on the sensor matrix used. They consist of a LYSO:Ce monolithic block, of 10 mm thickness and surface dimensions that match the total size of the corresponding matrix of sensors (Table 1). The light yield of the LYSO:Ce was set to 32000 ph/MeV and the crystals were coated with a diffuse reflector. The simulated sensor matrices for the optical readout were:

- Two matrices of 4x8 APDs (Hamamatsu S8550-02), [6].
- Four matrices of 4x4 SiPMs (SenL_Array2), [7].
- Four matrices of 4x4 Multi-Pixel Photon Counter (MPPC, Hamamatsu_S11828-344M), [6].

In all cases, a flat source of 511 keV photons was placed close to the entrance face of the block and gammas were emitted perpendicularly to the aforementioned face (Fig. 1 rigth). A high enough number of photons had to be sent from the flat source in order to have approximately 500 interacting photons per mm². Only 300 of these interacting gammas were subsequently used in the block training. The remaining 200 events configure the test data set which allows us to check the quality of the detector device. Moreover, only the photons that deposited more than 350 keV into the crystal were considered as valid events. The simulation output file contains the number of optical photons that reach each sensor, the total energy deposited into the crystal by the original gamma and its entrance point into the block.

The suitability of the described devices for our system can be affected, not only by the physical properties of each sensor, but also by the pixel dimensions and dead space between them. As a consequence we have evaluated two cases. Firstly, in the ideal case, we consider the raw data of optical photons that reach the pixels, and work under the assumption that all of them are individually detected. Secondly, we implement a more realistic case, which includes detection efficiency and noise effects of the devices. In this non-ideal case, the parameters involved in the readout data are not the same for all the sensors. A compilation of the values used is shown in Table II.

III. DETECTION EFFICIENCY AND NOISE EFFECTS

In order to implement the realistic case we should choose a suitable model that includes the detection efficiency of each sensor, and that emulates the contribution of the internal and electronic noise of each device. This model has to be necessarily different for the two types of sensors under study.

In the APD readout the number of detected photons should be reduced due to the quantum efficiency (QE) of the device. Moreover, since the APD internal gain is very low, the preamplifier noise has to be included in the analysis. Therefore, the number of optical photons that reach each pixel is multiplied by the QE and then the noise is included as an additive factor. The value of the noise factor is randomly generated into a normal distribution centered at 0 and with variance [8]:

$$\sigma^2 = N_\gamma \cdot QE \cdot (ENF - QE) + \left(\frac{ENC}{G}\right)^2 \qquad (1)$$

where N_γ is the number of optical photons that reach the pixel, ENF is the excess noise factor, ENC is the equivalent noise charge of the preamplifier and G the internal gain of the APD.

In the SiPMs case, the number of photons should be scaled with the photo detection efficiency (PDE) instead of QE. The PDE is a function of the QE of the active area, the ratio of active area with respect to the total area (geometrical fill factor, ε) and the triggering probability $P_{Trigger}$ [9]. In addition,

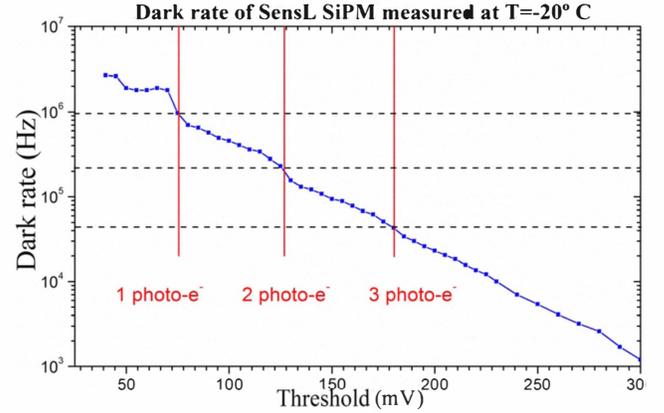| APDs	SiPMs
$QE = 70\ \%$	$\upsilon_{\text{dark counts}} \simeq 8$ MHz
$ENF = 1.75$	$ENF = 1.1$
$ENC = 700$ e⁻ rms	PDE (SensL) = 5, 10 %
$G = 100$	PDE (Ham.) = 50 %

Fig. 2. Dark rate of one pixel of the SensL matrix, measured at T=-20ºC. This plot allows to estimate the probabilities of firing several microcells with one electron.

the gain factor of the SiPMs is typically high enough ($G > 10^6$) to justify the simplification of the previous expression of the noise variance to the following one:

$$\sigma^2 \approx N_\gamma \cdot PDE \, (ENF - PDE) \qquad (2)$$

Furthermore, since the signal provided by a thermally generated electron and by a photo-generated one is the same in these devices, we should include a term of equivalent dark counts. Thermal electrons are assumed to be generated following a Poisson distribution. Therefore, the probability of measuring k electrons thermally generated during an interval δt is:

$$p(k) = \frac{e^{-\lambda} \cdot \lambda^k}{k!} \qquad (3)$$

where λ is the expected number of occurrences in δt, given by $\lambda = \upsilon_{dark\,counts} \cdot \delta t$, and $\upsilon_{dark\,counts}$ is the dark count rate of the device.

One of the parameters to be set before carrying out this work is the time interval δt. When the SiPMs are used as sensors it is important to know how long is the interval of time required before the digitalization process. The signals of the cells which fire with a dark count during δt are added to the measured pulse. Based on our current BrainPET prototype we assume that this time includes the generation of scintillation light in the crystal, the trigger formation, the coincidence time window and the time that the electronics requires to find this

	1 cell	2 cells	3 cells	>3 cells
SensL	76.1 %	19 %	3.7 %	1.2 %
Hamamatsu	50 %	20 %	15 %	0.2 %

	APDs Hamamatsu	SiPMs SensL
FWHM (mm)	0.66 ± 0.01	0.68 ± 0.03
FWTM (mm)	2.24 ± 0.03	1.91 ± 0.12

coincidence. We use our BrainPET prototype as reference system just in order to know the time interval that δt represents. However, δt will depend on the coincidence logic and electronics that have to be implemented in the future system.

In addition, we have to consider the optical crosstalk between cells. When an avalanche process takes place in one microcell, some of the secondary photons which are produced inside have the possibility of escaping to neighboring microcells and produce new avalanches in them. In spite SiPMs manufacturers have made an effort to minimize the cross talk by isolating the microcells as much as possible, this effect has not been totally corrected yet.

In order to evaluate the cross talk probabilities of the devices under study, we have measured the dark rate of one individual pixel of the simulated matrices. Since the probability of two simultaneous cells firing during the measuring time of the individual signal (few ns) is almost negligible (less than 0.3 % for 10 ns), we can assume that the counts whose amplitude corresponds to two or three optical photons are due to cross talk between cells (Fig. 2). The dark noise spectrum was measured at low temperature, due to the high dark rate that the devices present at room temperature. We work under the assumption that, although the absolute value of the dark rate depends on the temperature, the optical cross talk probability can be extrapolated from these measurements to room temperature case. Therefore, each primary cell firing has to be weighted with the probability of cross talk that we have measured for the corresponding sensor. The probabilities of firing one or more microcells with just one electron are shown in Table III.

IV. RESULTS

The global spatial resolution was estimated as the full-width-at-half-maximum (FWHM) and the full-width-at-tenth-maximum (FWTM) of the total error distribution, which includes positions over the entire block. Besides, local error distributions in positions along each axis provide information about the detector linearity. All the results showed in this section are mean values, with its standard deviations, of three independent training procedures of the devices.
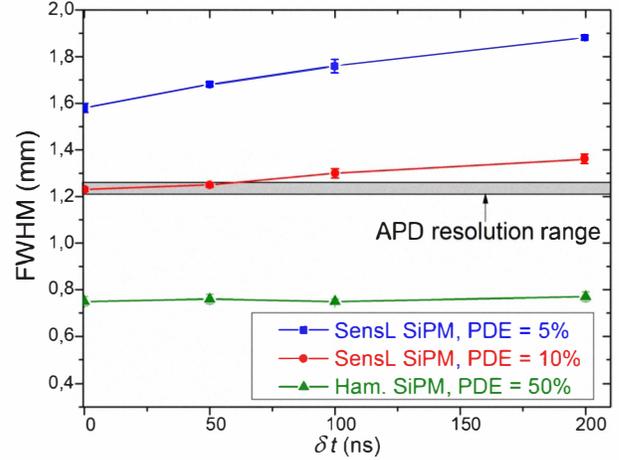

Fig. 3. Dependence of the spatial resolution of the SiPMs with different *PDE* on the "time before digitalization", δt. The range of resolutions provided by the APDs is shown in grey.

	FWHM (mm)	FWTM (mm)
APDs ($QE = 70$ %)	1.23 ± 0.01	3.50 ± 0.02
SiPMs SensL (PDE = 5 %)	1.68 ± 0.01	4.15 ± 0.02
SiPMs SensL (PDE = 10 %)	1.25 ± 0.01	3.19 ± 0.02
SiPMs Ham. (PDE = 50 %)	0.76 ± 0.02	2.25 ± 0.02

A. Ideal Case

In the ideal case the position is calculated from the raw data of number of optical photons. This way only the geometrical effects are taken into account and the noise and sensor efficiencies are ignored. Under these ideal conditions the results obtained are comparable for both devices. It can be observed in Table IV that the hypothetical negative effect derived from the bigger size of the SiPM pixels (aprox. 3 mm × 3 mm) compared with APDs (1.6 mm × 1.6 mm) resulted to be totally negligible.

B. Non-Ideal Case

In order to evaluate the non-ideal case we have to take into account the sensor efficiencies and the previously described noise model. The parameters that have been used for this non-ideal model are collected in Table II. Most of these values have been extracted from the devices' datasheets [6], [7]. In the Hamamatsu MPPC case, a *PDE* of 50 % is specified for 440 nm wavelength, which is close to the LYSO:Ce emission peak (420 nm). On the other hand, the SensL SiPM datasheet details values from 10 to 20 % *PDE* for 520 nm. For this reason we chose to simulate two different values, 5 and 10 % *PDE*, which have to be lower than the specified ones because our wavelength is 420 nm.

Several values of δt have been tested. Fig. 3 shows the behaviour of the spatial resolution FWHM as a function of the time δt for all the simulated devices. The range of values provided by the APD case, close to 1.2 mm, is shadowed in
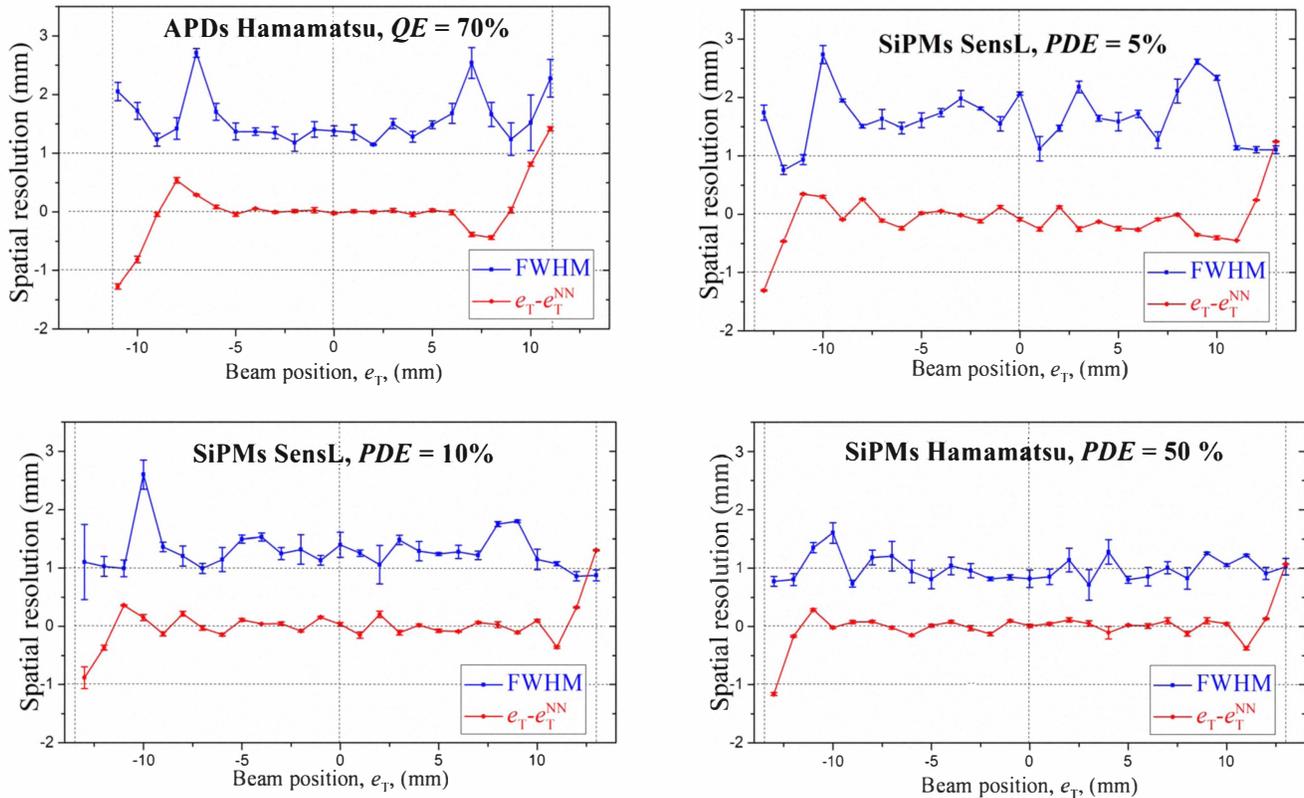
Fig. 4. Local resolution and non-linearity along the transversal axis under non-ideal conditions for all the simulated sensors. In all cases the noise was simulat with $\delta t = 50$ ns. APDs of Hamamatsu (top-left), SiPMs of SensL with 5% of PDE (top-right), SiPMs of SensL with 10 % of PDE (bottom-left) and SiPMs Hamamatsu with 50% of PDE (bottom-right.).

grey. Since the number of dark counts added to the signal increases with δt, we observe that for sensors with low *PDE* the spatial resolution FWHM worsens for longer δt values.

In Table V are shown the spatial resolution FWHM and FWTM obtained for the different matrices, with δt set at 50 ns. In the SiPMs cases, both resolution values show a strong dependence on the device efficiency. In fact, only devices with a *PDE* higher than 10 % provide better spatial resolution results than the APD matrices. In Fig. 4 is represented the spatial resolution (FWHM) and the mean deviation with respect to the real position $(e_T - e_T^{NN})$ at 1 mm steps along the transversal axis of the blocks. It can be observed that the local resolution values become smaller and more uniform over the entire axis for SiPMs devices with higher *PDE*.

We can extract from these results that noise effects are almost corrected by the neural network algorithms if the *PDE* is high enough, but they become important and lead to wrong estimations if the number of optical photons detected is low.

V. CONCLUSIONS

SiPMs seem to be a good alternative to APDs in the readout of monolithic blocks, as one would expect. The geometrical negative effect derived from the bigger size of the SiPMs pixels compared with APDs shows not to be noticeable. In the other hand, SiPMs present similar resolution capabilities (or even better if we use high *PDE* devices) and

they are faster, more robust and easier to work with due to their higher internal gain. The selection of a SiPM sensor with the higher possible *PDE* for the desired wavelength (420nm) arises as a critical issue from this study, in order to improve the performance of the APD-based detector design

REFERENCES

[1] P. Rato Mendes et al., "Design and Prototyping of a Human Brain PET Scanner Based on Monolithic Scintillators," *2010 IEEE Nuclear Science Symp. Conf. Rec.*, 2010, pp. 2798-2800.
[2] P. Garcia de Acilu, et al., "Study and optimization of positioning algorithms for monolithic PET detectors blocks," *JINST - 9th International Conference on Position Sensitive Detectors, PSD9*, Sept. 2011. [in press].
[3] P. Rato Mendes et al. "Optimization of a monolithic detector block design for a prototype human brain PET scanner," *2008 IEEE Nuc. Sci. Symp. Conf. Rec.*, 2008, pp. 4927-4930.
[4] I Sarasola et al., "PET demonstrator for a human brain scanner based on monolithic detector blocks," *Trans. Nuc. Sci.*, vol. 58, no. 5, pp. 2190-2197, Oct. 2011.
[5] P. Arce et al. "GAMOS: a GEANT4-based easy and flexible framework for nuclear medicine applications," *2008 IEEE Nuc. Sci. Symp. Conf. Rec.*, 2008, pp. 3162-3168.
[6] Hammamatsu Photonics [Online] Available:
 http://jp.hamamatsu.com/products/sensor-ssd/index_en.html

[7] SenL [Online] Available:
http://sensl.com/products/silicon-photomultipliers/
[8] H. H. Barrett and K. Myers, *Foundations of image science, Wiley–Interscience*, 2003.
[9] D. Renker and E. Lorenz, "Advances in solid state photon detectors," *JINST,* vol. 4, no. 4, P04004, Apr. 2009.